Fluid flow-based description of the geometrical features in fluidic channels using the Shannon's information theory: an exploratory study

(Article begins on next page)

16 April 2024

2

3   Brief Communication

4

5   **Fluid flow-based description of the geometrical features in fluidic channels using the Shannon's**

6   **information theory: an exploratory study**

7

8   S. Ripandelli[1*], D. Pugliese[2*], M. Sotgiu[1], U. Morbiducci[1]

9   [1]Politecnico di Torino, Department of Mechanical and Aerospace Engineering, 10129 Torino,

10   Italy

11   [2]Politecnico di Torino, Department of Applied Science and Technology and RU INSTM, 10129

12   Torino, Italy

13

14   *corresponding authors: simone.ripandelli@gmail.com; ORCID: 0000-0001-7867-9461

15   diego.pugliese@polito.it; ORCID: 0000-0002-6431-1655

16

17   Keywords

18   Shannon Entropy, microfluidics, information theory, thermodynamics, fluids

19

20   **Abstract**

21   Inspired by Nature, where storing information is an intrinsic ability of natural systems, here we

22   investigate the capability of interacting systems to transport/store the information

23   generated/exchanged in the interaction process in the form of energy or matter, preserving it

24   over time. In detail, here we test the possibility to consider a fluid as a carrier of information,

25   speculating about how to use such information. The final goal is to demonstrate that

26   information theory can be used to illuminate physical observations, even in those cases where

27   the equations describing the phenomenon under investigation are intractable, are affected by

28   a budget of uncertainty that makes their solution not affordable or may not even be known. In

29   this exploratory work an information theory-based approach is applied to microfluidic data. In

30   detail, the classical study of the fluid flow in a microchannel with obstacles of different

31   geometry is faced by integrating fluid mechanics theory with Shannon's theory of information,

32   interpreted in terms of thermodynamics. Technically, computational fluid dynamics

33   simulations at Reynolds' numbers (*Re*) equal to 1 and 50 were carried out in fluidic channels

34   presenting obstacles with rectangular and semicircular shape, and on the simulated flow fields

35 the Shannon's information theory was applied evaluating the fluid dynamics information

36 entropy content. It emerged that the Shannon Entropy (SE) evaluated at the outflow section of

37 the flow channel depends upon the geometric features (i.e. position, shape, aspect ratio) of the

38 obstacles. This suggests an interpretation of the fluid dynamics establishing in a flow channel

39 presenting obstacles in terms of information theory, that can be used to identify *a posteriori*

40 the geometric features of the obstacles the fluid interacts with. The proposed approach can be

41 applied to flow data at the boundaries of fluid domains of interest to extract information on the

42 process occurring inside a system, do not making any appeal to the governing equations of the

43 phenomenon under observation or intrusive measurements.

44

45 **1 Introduction**

46 In principle, the behavior of fluids in motion can be fully described by three equations: an

47 equation describing the conservation of mass, a second equation based on the second Newton's

48 law of motion, and a third equation based on the conservation of energy (Cox 2015; Khasanov

49 2011; Merdasi et al. 2018).

50   A condition for a real fluid to be in motion is that sufficient energy is to be spent. It follows

51 that the fluid in motion is a system that modifies its internal energy, thus generating a variation

of entropy (S) of the system in a purely thermodynamic meaning. The concept of entropy (not

univocally accepted indeed), which can be explained as the level of disorder of a system

describing its evolution under the effect of the external environment, was taken up by Claude

Shannon in 1948 (Shannon 1948) and applied to the field of information theory in order to

describe the level of complexity of a signal in data communication systems. In general, it is still

uncommon to apply information theory for the purpose of the analysis of flow fields

characterized by different levels of complexity (Ikeda and Matsumoto 1986). Indeed, the idea

of considering a fluid in motion as an information carrier is not new, inspired by the fact that

Nature uses fluids to transport a plethora of biochemicals. Looking at a fluid in motion as an

information carrier (e.g. nutrients to cells, proteins through blood, etc.), a parallelism between

fluid flow and information theory based on the definition of the SE can be easily established.

   Motivated by the possibility of interpreting a fluid as information carrier, in this study

information theory is applied to microfluidics, where its capability to discriminate the shape of

obstacles in a channel based on the knowledge of the motion of fluid particles upstream and

downstream of the obstacle is tested. In detail, the capability of the SE to discriminate the shape

of the obstacle based on the distortion of fluid streamlines is tested, with the final aim to use

the SE of the system as a *fingerprint* of the obstacle shape-specific flow perturbation. The

4

69   potency of the herein proposed approach has not been largely explored. To cite a valuable

70   example, Pozo et al. (Pozo et al. 2017) analyzed the flow complexity in open systems,

71   approaching the distortion of fluid streamlines in a channel at the level of information

72   transmission.

73   Technically, here computational fluid dynamics (CFD) solutions of laminar flow in channels

74   presenting obstacles were compared to an "ideal communication" channel where the

75   transmitted and received messages are identical and SE was applied to CFD data. The

76   characterization of microflows as information carriers finds several applications, e.g. to assess

77   mixing efficiency in micromixers (Camesasca et al. 2006; Pennella et al. 2010; Pennella et al.

78   2012) or in microreactors and in scaffolds and bioreactors for tissue engineering applications

79   (Eijkel and Van den Berg 2005; Bilen and Yapici 2002; Yojina and Ngamsaad 2010; Tariq et al.

80   2020) and in many other technological fields like solar energy (Ali 2020), nanofluids for

81   manufacturing processes (Wang et al. 2020), heat and mass transfer (Chen et al. 2020; Sajjad

82   et al. 2020; Sözen et al. 2021).

83   The principal aim of this study, and the reason of its novelty, was to investigate the behavior

84   of a fluid that flows in a channel in presence of obstacle/s characterized by different shape,

85   multiplicity and disposition and employing the information theory. This exploratory study

86   highlights that at defined conditions a simplified approach based on the information theory can

87   be applied to extract information on the processes occurring within closed systems, and that

88   this can be done by measuring only the "information" at systems' boundaries.

89

90   **2 Methods**

91   In this study a microchannel geometry without and with obstacles of different shape and

92   position was investigated. Overall, as depicted in Fig. 1, nine configurations were considered,

93   i.e. one without obstacles and 8 with obstacles. The ratio between the height of the channel h_{ch}

94   and the characteristic obstacle dimension h_1 was set to $h_1 = h_{ch}/6$. In microchannel

95   configurations where more than one obstacle was considered, inter-distance was set equal to
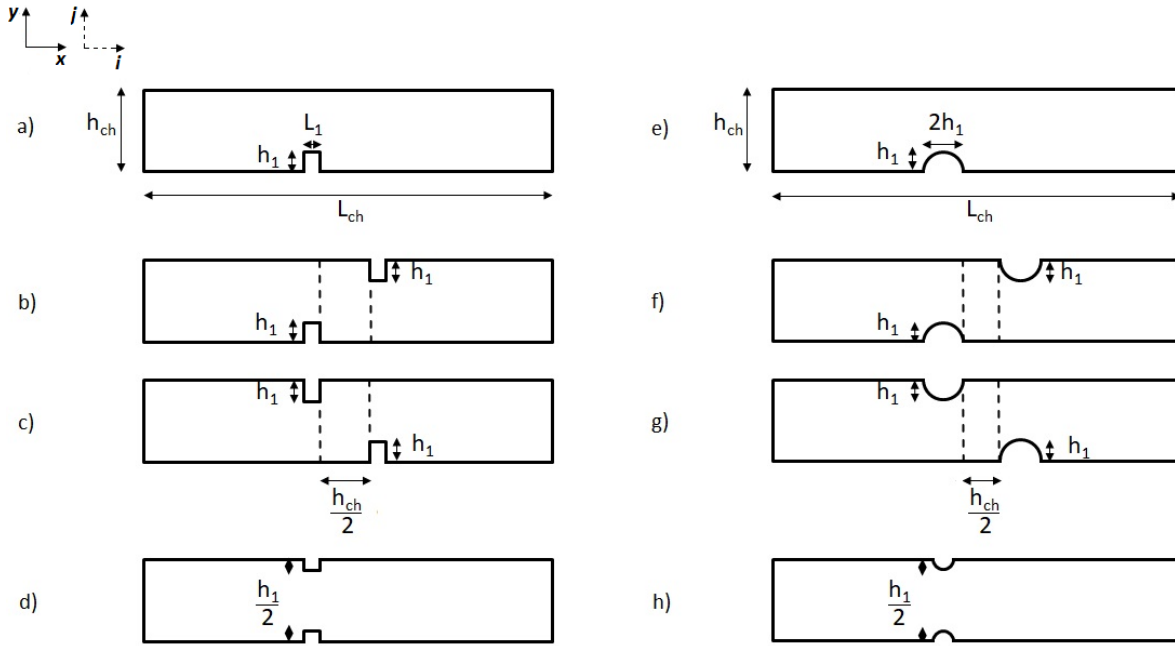
96     $h_{ch}/2$ (Fig. 1).

97

98   **Fig. 1** Schematic illustration of the investigated channel geometries with obstacles ($h_1 = h_{ch}/6$). The

99   analysis on models a, d, e and h is presented in the Results Section. Coordinates (i, j) correspond to the

100   logical coordinates useful for the computational analysis

101 The analytical solution of the fluid motion in the microchannel without obstacles can be easily

102 obtained from Navier-Stokes equations. In detail, for an incompressible, homogeneous,

103 Newtonian fluid in steady-state laminar condition, the law of motion in the microchannel can

104 be expressed as:

$$u_x = -\frac{1}{2\mu} \cdot \frac{dp}{dx} \cdot (y_0^2 - y^2) \ (1)$$

106 where u_x is the velocity in axial (x, see Fig. 1) direction, μ the dynamic viscosity, p the pressure,

107 y the general position in vertical direction (Fig. 1) and y_0 the coordinate of the microchannel

108 wall, where velocity is equal to 0 (i.e. no-slip conditions).

109 The finite volume-based CFD commercial code Fluent (ANSYS Inc., USA) was adopted to solve

110 the discretized governing equations of fluid motion in microchannels with obstacles. In detail,

111 the Navier-Stokes equations in their discretized form and under steady-state laminar

112 conditions were solved using a second order pressure discretization and a second order

113 upwind momentum discretization scheme. The fluid was assumed to be isotropic,

114 incompressible and Newtonian with a density value ρ equal to 998.2 [kg·m^{-3}] and a dynamic

115 viscosity μ equal to 10^{-2} [kg·s·m^{-2}]. To ensure grid-independence of the solution, based on a

116 mesh sensitivity analysis, quad-mesh with elements size of $1·10^{-4}$ m was adopted. On average,

117 the resulting computational grids consisted of 24000 elements and 24381 nodes. Two different

8

118   flow regimes, characterized by *Re* equal to 1 and 50, were simulated by applying Dirichlet

119   conditions at the inflow section of the microchannel geometry (in terms of flat velocity profile),

120   while the reference pressure Neumann boundary condition was imposed at the outflow section.

121   Walls were assumed to be rigid, and the no-slip condition was imposed.

122   The concept that a confined fluid in motion is an information carrier, and the parallel with a

123   communication system, was translated into a scheme where: (1) the fluid in the microchannel

124   is the carrier; (2) the inflow section (or more in general a section upstream of the channel

125   segment presenting obstacles) is the transmitter; (3) the outflow section (or more in general a

126   section downstream of the channel segment presenting obstacles) is the receiver; (4) the

127   difference in flow features between the two sections is the information transmitted. In this

128   regard, flow perturbations induced by the presence of obstacles can be regarded as the "noise"

129   affecting the system (Fig. 2). The channel without obstacles was considered as the reference

130   case, i.e. the case where the carrier (fluid) is not disturbed and the transmitted information is

131   not modified.

132

133
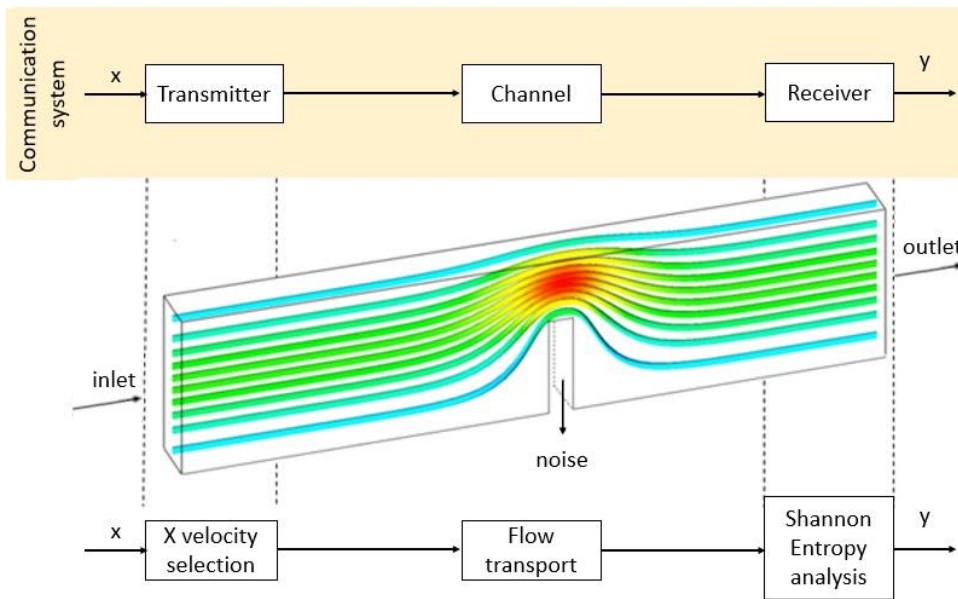
134

135 **Fig. 2** Schematic illustration of the parallelism between a communication system and a fluidic system

136 Distilling in fluid mechanics terms, at the very low Re laminar flow regimes adopted in

137 microfluid applications the streamlines deflection induced in the channel by the presence of an

138 obstacle does represent a modification of the information content carried by the fluid at any

139 channel location upstream of the obstacle. In the absence of obstacles, fluid streamlines will not

140 be deflected, following a linear path; any obstacle capable to perturb the flow will deflect fluid

141 streamlines and ultimately the carried information, in accordance with the conceptual model

142 of Fig. 1. It is well known from the analytical solution of the laminar fluid motion in the channel

143 without obstacles, that the flow field is characterized by streamlines parallel to the axis of the

144 conduit (as well as to the channel's walls). The presence of an obstacle, even maintaining

145   laminar conditions, will perturb the flow with the consequence that streamlines will be

146   deflected losing their parallelism. This behavior was translated building up a binary matrix,

147   representative of the phenomena. To build up the representative binary matrix, here fluid

148   velocity data from CFD simulations were considered (i.e. for each cell of the quad-mesh a value

149   of velocity was extrapolated). Technically, a $N \times M$ matrix $B_{i,j}^x$ was built:

150
$$B_{i,j}^x = \begin{bmatrix} b_{1,1} & \dots & b_{1,M-1} \\ \vdots & \ddots & \vdots \\ b_{N,1} & \dots & b_{N,M-1} \end{bmatrix} \qquad (2)$$

151   with $i = \{1, \dots N\}$, where N is the number of grid cells in y direction, and $j = \{1, \dots M - 1\}$, where

152   M is the number of grid cells in x direction (Fig. 1). The binary elements $b_{i,j}$ of the matrix were

153   calculated as follows:

154
$$b_{i,j} = \begin{cases} 1, & \frac{\bar{u}_{i,j}^x}{\bar{u}_{i,j-1}^x} \leq \zeta_{i,j} \\ 0, & otherwise \end{cases} \qquad (3)$$

155   where $\bar{u}_{i,j}^x$ and $\bar{u}_{i,j-1}^x$ are the values of the x-component of the velocity at grid cell location (i, j)

156   and $(i, j\text{-}1)$, respectively. The threshold values $\zeta_{i,j}$ for matrix $B_{i,j}^x$ binarization were set according

157   to:

158
$$\zeta_{i,j} = \frac{\bar{u}_{i,j}^{num.}}{\bar{u}_{i,j-1}^{num.}} - \frac{\bar{u}_{i,j}^{ana.}}{\bar{u}_{i,j-1}^{ana.}} = 0 \qquad (4),$$

159

160   and depend on the results of CFD analysis and Eq. (1). From this equation, $\bar{u}_{i,j}^{num.}$ and $\bar{u}_{i,j}^{ana.}$ are

161   the CFD and the analytical velocity values in x direction at grid cell location (i, j), and $\bar{u}_{i,j-1}^{num.}$ and

162    $\bar{u}_{i,j-1}^{ana.}$ are the CFD and the analytical velocity values in x direction at grid cell location (i, j-1),

163   respectively.

164   Here the SE was employed to quantify the level of interaction between fluid flow and the

165   obstacles in the microchannel, intended as the level of streamlines deflection with respect to

166   the microchannel without obstacles, binarized according to matrix $B_{i,j}^{x}$. By definition, the

167   formulation of the SE is given by:

168 $SE(X_i) = -P(X_i)\, log_2\, P(X_i)$ 				(5),

169   where X_i is a discrete random variable with possible values $\{X_1, ..., X_n\}$ and $P(X_i)$ is the

170   probability distribution of X_i. Theoretically, an increase of entropy corresponds to a loss in

171   information content. In this study, the SE was evaluated according to:

172 $SE = -P_i\, log_2\, P_i$ 				(6)

173   where P_i is given by:

174 $P_i = \dfrac{\sum_1^j b_{i,j}}{N}$ 				(7)

175   Based on Eqs. (6) and (7), the SE ranges between zero (i.e. no information lost or, for the

176   specific application, no distortion of fluid streamlines) and one (i.e. all the information carried

12

177   by the fluid lost due to the disruption of the flow field as a consequence of its interaction with

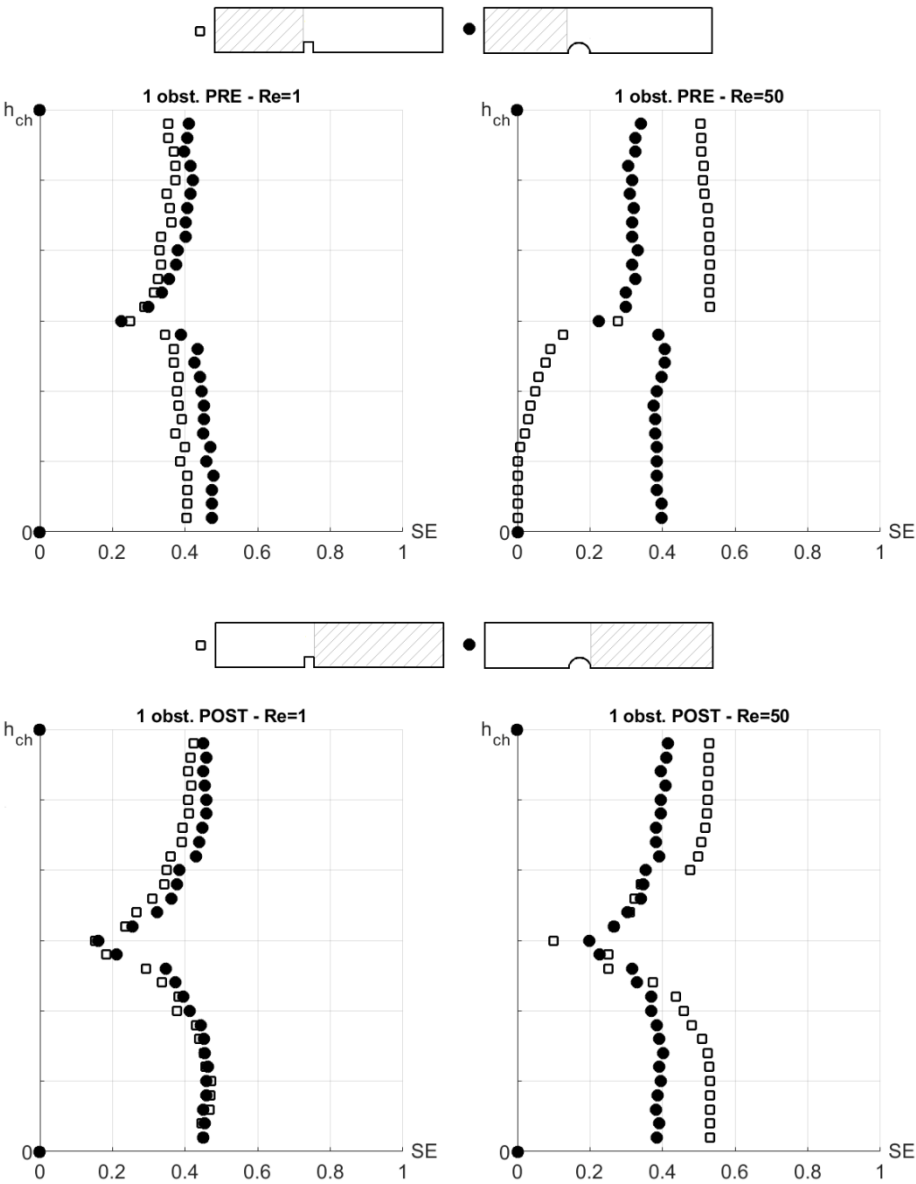178   obstacles in the microchannel).

179

180   **3 Results**

181   The analysis was extended to all the microchannels with different obstacles geometry and

182   number summarized in Fig. 1. As first explanatory example, the SE values computed along two

183   cross-sections (proximal and distal to the obstacle, respectively) of the two microchannels with

184   single obstacles of rectangular and semicircular shape, at two different Re numbers (1 and 50),

185   are presented in Fig. 3. At $Re = 1$, as expected, moderate differences are highlighted by the SE

186   both between the upstream and downstream sections (flow field distortion consequence of the

187   presence of the obstacle) and between the two microchannels (consequence of the different

188   shape of the obstacles). Marked differences in SE distribution (and in absolute values as well)

189   along the cross-sections emerge at $Re = 50$ (Fig. 3): as expected, the presence of the rounded

190   (semicircular) obstacle, which is expected to distort fluid streamlines less than the obstacle

191   with rectangular shape, modifies trans-obstacle SE values markedly less than the rectangular

192   single obstacle (the semicircular shape maintains almost unaltered the SE of the system even

193   increasing the inertial effects by one order of magnitude, as stated by the Re). The results of Fig.

194   3 confirm the capability of the SE of discriminating between obstacle shapes, properly

195   capturing thermodynamically-induced variations in the microchannel system.
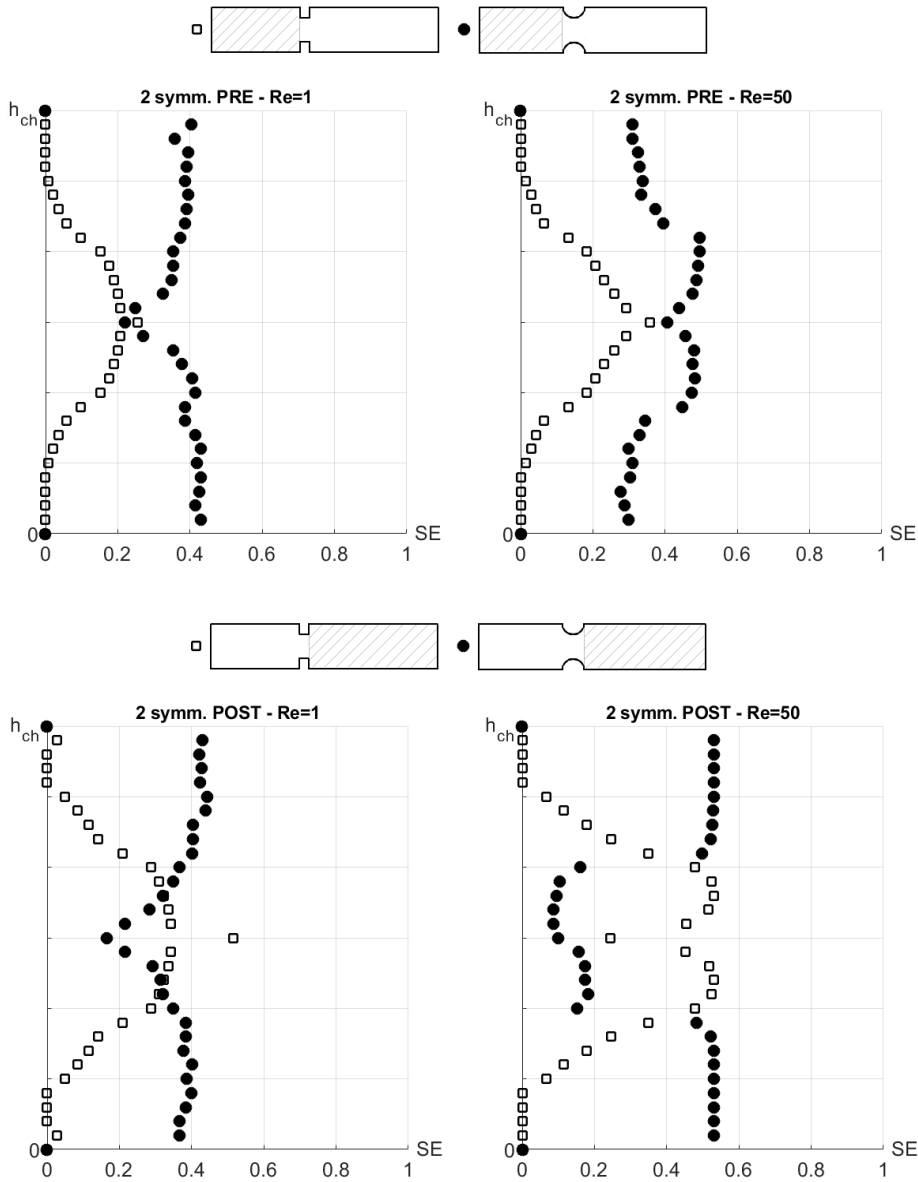

197   **Fig. 3** SE computed on two cross-sections (proximal to the obstacle, upper panel; distal to the obstacle,

198   lower panel) of two microchannels presenting single obstacles with different shape (rectangular and

199   semicircular), at two different *Re* (1 and 50). h_{ch} is the general height of the channel

200   Figure 3 also highlights an expected lack of symmetry (more pronounced at $Re = 50$) in the SE

201   cross-sectional distribution, reflecting the absence of geometrical and fluid dynamical

202   symmetry in the two microchannels with single obstacles. In this regard, the second

203   explanatory example of Fig. 4 reports the SE values computed along two cross-sections

204   (proximal and distal to the obstacle, respectively) of the two microchannels presenting

205   obstacles with rectangular and semicircular shape, symmetrically located with respect to the

206   microchannel axis. In this case, the cross-sectional SE distributions: (1) confirm the capability

207   of capturing the different influence of the shape of the obstacle in the flow field, with marked

208   differences related to the obstacle shape clearly evident also at $Re = 1$; (2) adequately reflect

209   the presence of a geometrical (and fluid dynamical) symmetry of the microchannel system.

210   Summarizing, the cross-sectional distributions of Figs. 3 and 4 clearly demonstrate that SE

211   is an indirect measure of the impact that obstacles with different shape and configuration have

212   on the microchannel fluid dynamics, suggesting that SE can be adopted to *a posteriori*

213   discriminate the shape of obstacles (e.g. cultured cells in biomicrofluidic applications) in

214   systems without optical access. This is like to say that SE can be used as a sort of *fingerprint*

215   that specific obstacles leave on fluid streamlines, depending upon their shape, configuration

216   and fluid dynamics conditions (as defined by the Reynolds' number).

217

Fig. 4 SE computed on two cross-sections (proximal to the obstacle, upper panel; distal to the obstacle,

lower panel) of two microchannels presenting obstacles with rectangular and semicircular shape, at *Re*

= 1 and 50. Obstacles are symmetrically located with respect to the axis of the microchannels. h_{ch} is the

general height of the channel.

223   In order to check for the robustness of SE with respect to the CFD grid cardinality (i.e. the

224   number of nodes considered for the SE calculation), a sensitivity analysis was carried out where

225   nodes were decimated. Technically, the average value of the SE was calculated considering the

226   entire microchannel fluid domain as follows: (1) considering the 100% of the mesh grid

227   elements; (2) considering only 50% of the mesh grid elements; (3) averaging the velocity

228   values of two adjacent mesh grid elements. The percentage differences among the average SE

229   values, summarized in Fig. 5 for microchannels with four different semicircular shape obstacle

230   configurations, clearly show that a substantial reduction (50%) in the number of mesh grid

231   elements weakly influences SE evaluation (with differences lower than 6%).

232
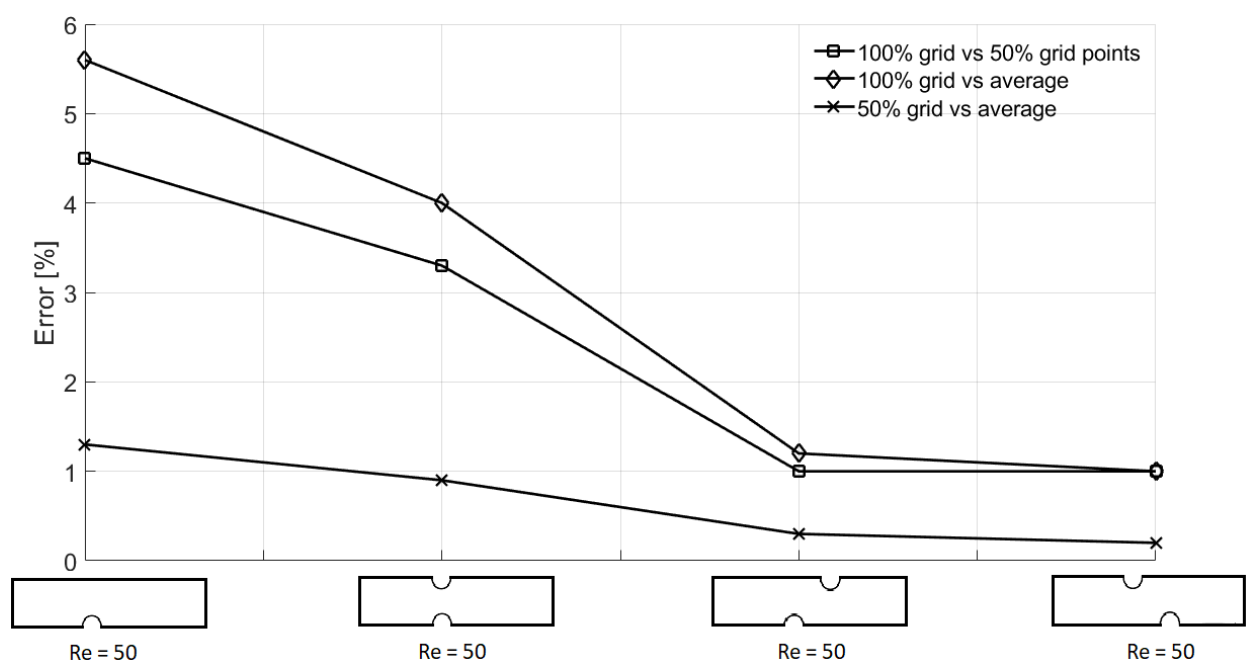
233   **Fig. 5** Impact of the number of mesh grid elements on microchannel average SE values. The analysis was

234   carried out considering the 100% and the 50% of the mesh grid elements, as well as averaging the

235 velocity values of two adjacent mesh grid elements. The results refer to four microchannels with

236 different configurations of semicircular obstacles

237

238 **4 Conclusions**

239 In this study the fluid dynamics in microchannels with obstacles was investigated using the

240 concept of entropy, here approached in a different way compared to the present state-of-the-

241 art (Camesasca et al. 2006, Pozo et al. 2017, Rocha et al. 2008). The analysis suggests that a

242 quantity linked to entropy, SE, is capable to discriminate among different shapes and

243 configurations of obstacles within a microchannel. In the microfluidic field the capability to

244 infer presence and configuration of obstacles in microsystems from SE differences between

245 inflow and outflow sections could allow to monitor e.g. cells shape and growth in

246 microbioreactors, as well as mixing of species in the microsystem itself. Applications other than

247 biomicrofluidics, where fluid streamlines entropy can be employed to describe the physics

248 within the microsystem just looking at SE input and output variations are manifold, ranging

249 from microelectronics to chemistry (Ghaneifar et al. 2021, Shahsavar et al. 2020, Khalid et

250 al. 2021). In this sense, the here presented results represent a starting point for future

251 dedicated applications where the extraction of information on the processes occurring inside a

252 not accessible system is critical.

253 Integrating statistical mechanics with information theory, in the long run will allow to

254 establish a clearly distinguishable link between thermodynamics perturbation of a system and

255 the level of interaction of the individual elements of which a system is made.

256

Conflicts of interest

258 The authors declare that they have no competing interests.

259

References

261 Ali HM (2020) Recent advancements in PV cooling and efficiency enhancement integrating

262 phase change materials based systems – A comprehensive review. Sol Energy 197:163–

263 198. https://doi.org/10.1016/j.solener.2019.11.075

264 Bilen K, Yapici S (2002) Heat transfer from a surface fitted with rectangular blocks at different

265 orientation angle. Heat Mass Transfer 38:649–655.

266 https://doi.org/10.1007/s002310100275

267 Camesasca M, Kaufman M, Manas-Zloczower I (2006) Quantifying fluid mixing with the

268 Shannon   entropy.   Macromol   Theory   Simul   15:595–607.

269 https://doi.org/10.1002/mats.200600037

270 Chen C-Y, Su J-H, Ali HM, Yan W-M, Amani M (2020) Effect of channel structure on the

271 performance of a planar membrane humidifier for proton exchange membrane fuel cell. Int

272 J   Heat   Mass   Transfer   163:120522.

273 https://doi.org/10.1016/j.ijheatmasstransfer.2020.120522

274 Cox SJ (2015) Simulations of bubble division in the flow of a foam past an obstacle in a narrow

275 channel. Colloids Surf, A 473:104–108. https://doi.org/10.1016/j.colsurfa.2014.10.038

276 Eijkel JCT, van den Berg A (2005) Nanofluidics: what is it and what can we expect from it?

277 Microfluid Nanofluid 1:249–267. https://doi.org/10.1007/s10404-004-0012-9

278 Ghaneifar M, Raisi A, Talebizadehsardari P (2021) Mixed convection heat transfer of Al_2O_3

279 nanofluid in a horizontal channel subjected with two heat sources. J Therm Anal Calorim

280 143:2761–2774. https://doi.org/10.1007/s10973-020-09887-2

281 Ikeda K, Matsumoto K (1989) Information theoretical characterization of turbulence. Phys Rev

282 Lett 62:2265–2268. https://doi.org/10.1103/PhysRevLett.62.2265

283   Khalid SU, Babar H, Ali HM, Janjua MJ, Ali MA (2021) Heat pipes: progress in thermal

284   performance enhancement for microelectronics. J Therm Anal Calorim 143:2227–2243.

285   https://doi.org/10.1007/s10973-020-09820-7

286   Khasanov NA (2011) Acoustic oscillations of a gas near nested thin-walled cylindrical obstacles

287   in   a   channel.   J   Appl   Mech   Tech   Phys   52:577–584.

288   https://doi.org/10.1134/S0021894411040109

289   Merdasi A, Ebrahimi S, Moosavi A, Shafii MB, Kowsary F (2018) Simulation of a falling droplet

290   in a vertical channel with rectangular obstacles. Eur J Mech B Fluids 68:108–117.

291   https://doi.org/10.1016/j.euromechflu.2017.11.002

292   Pennella F, Mastrangelo F, Gallo D, Massai D, Deriu MA, Falvo D'Urso Labate G, Bignardi C,

293   Montevecchi F, Morbiducci U (2010) A survey of microchannel geometries for mixing of

294   species in biomicrofluidics. In: Dias R, Lima R, Martins AA, Mata TM (eds.) Single and two-

295   phase flows on chemical and biomedical engineering, 1st edn. Bentham Science Publishers,

296   Sharjah, pp 548–578. https://doi.org/10.2174/978160805295011201010548

297   Pennella F, Rossi M, Ripandelli S, Rasponi M, Mastrangelo F, Deriu MA, Ridolfi L, Kähler CJ,

298   Morbiducci U (2012) Numerical and experimental characterization of a novel modular

299   passive micromixer. Biomed Microdevices 14:849–862. https://doi.org/10.1007/s10544-

300   012-9665-4

301   Pozo JM, Geers AJ, Villa-Uriol M-C, Frangi AF (2017) Flow complexity in open systems:

302   interlacing complexity index based on mutual information. J Fluid Mech 825:704–742.

303   https://doi.org/10.1017/jfm.2017.392

304   Rocha LB, Adam RL, Leite NJ, Metze K, Rossi MA (2008) Shannon's entropy and fractal

305   dimension provide an objective account of bone tissue organization during calvarial bone

306   regeneration. Microsc Res Tech 71:619–625. https://doi.org/10.1002/jemt.20598

307   Sajjad U, Sadeghianjahromi A, Ali HM, Wang C-C (2020) Enhanced pool boiling of dielectric and

308   highly wetting liquids - a review on enhancement mechanisms. Int Commun Heat Mass

309   Transfer 119:104950. https://doi.org/10.1016/j.icheatmasstransfer.2020.104950

310   Shahsavar A, Ali HM, Mahani RB, Talebizadehsardari P (2020) Numerical study of melting and

311   solidification in a wavy double-pipe latent heat thermal energy storage system. J Therm

312   Anal Calorim 141:1785–1799. https://doi.org/10.1007/s10973-020-09864-9

313   Shannon CE (1948) A mathematical theory of communication. Bell Syst Tech J 27:379–423.

314   https://doi.org/10.1002/j.1538-7305.1948.tb01338.x

315 Sözen A, Filiz Ç, Aytaç İ, Martin K, Ali HM, Boran K, Yetişken Y (2021) Upgrading of the

316   performance of an air-to-air heat exchanger using graphene/water nanofluid. Int J

317   Thermophys 42:35. https://doi.org/10.1007/s10765-020-02790-w

318 Tariq HA, Anwar M, Malik A, Ali HM (2020) Hydro-thermal performance of normal-channel

319   facile heat sink using TiO_2-H_2O mixture (Rutile-Anatase) nanofluids for microprocessor

320   cooling. J Therm Anal Calorim. https://doi.org/10.1007/s10973-020-09838-x

321 Wang X, Li C, Zhang Y, Ding W, Yang M, Gao T, Cao H, Xu X, Wang D, Said Z, Debnath S, Jamil M,

322   Ali HM (2020) Vegetable oil-based nanofluid minimum quantity lubrication turning:

323   Academic   review   and   perspectives. J   Manuf   Processes 59:76–97.

324   https://doi.org/10.1016/j.jmapro.2020.09.044

325 Yojina J, Ngamsaad W, Nuttavut N, Triampo D, Lenbury Y, Kanthang P, Sriyab S, Triampo W

326   (2010) Investigating flow patterns in a channel with complex obstacles using the lattice

327   Boltzmann method. J Mech Sci Technol 24:2025–2034. https://doi.org/10.1007/s12206-

328   010-0712-x